

Low-Valent Metal Ions as MOF Pillars: A New Route Toward Stable and Multifunctional MOFs

R. Eric Sikma, Naman Katyal, Su-Kyung Lee, Joseph W. Fryer, Catherine G. Romero, Samuel K. Emslie, Elinor L. Taylor, Vincent M. Lynch, Jong-San Chang,* Graeme Henkelman,* and Simon M. Humphrey*



Cite This: *J. Am. Chem. Soc.* 2021, 143, 13710–13720



Read Online

ACCESS |



Metrics & More

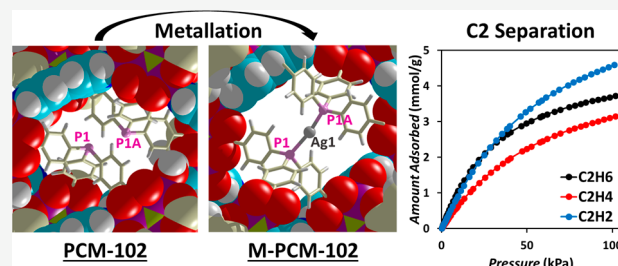


Article Recommendations



Supporting Information

ABSTRACT: PCM-102 is a new organophosphine metal–organic framework (MOF) featuring diphosphine pockets that consist of pairs of offset *trans*-oriented P(III) donors. Postsynthetic addition of M(I) salts (M = Cu, Ag, Au) to PCM-102 induces single-crystal to single-crystal transformations and the formation of *trans*-[P₂M]⁺ solid-state complexes (where P = framework-based triarylphosphines). While the unmetalated PCM-102 has low porosity, the addition of secondary Lewis acids to install rigid P–M–P pillars is shown to dramatically increase both stability and selective gas uptake properties, with N₂ Brunauer–Emmett–Teller surface areas >1500 m² g^{−1}. The Ag(I) analogue can also be obtained via a simple, one-pot peri-synthetic route and is an ideal sacrificial precursor for materials with mixed bimetallic M^A/M^B pillars via postsynthetic, solvent-assisted metal exchange. Notably, the M-PCM-102 family of MOFs contain periodic *trans*-[P₂M]⁺ sites that are free of counter anions, unlike traditional analogous molecular complexes, since the precursor PCM-102 MOF is monoanionic, enabling access to charge-neutral metal-pillared materials. Four M-PCM-102 materials were evaluated for the separation of C2 hydrocarbons. The separation performance was found to be tunable based on the metal(s) incorporated, and density functional theory was employed to elucidate the nature of the unusual observed sorption preference, C₂H₂ > C₂H₆ > C₂H₄.



INTRODUCTION

Metal–organic frameworks (MOFs)¹ that are permanently microporous and feature structurally well-defined, low-valent metal species inside the micropores are of topical interest for molecular separations² and heterogeneous catalysis.³ MOF functionalization with heavier low-valent metals that have radially expanded valence orbitals is likely to engender stronger host–guest binding interactions. In turn, this could enable greater sorption selectivity, higher Q_{st} values, and improved separation performance.⁴ In certain cases, such MOFs could be capable of achieving formal chemisorption of guest adsorbates and would therefore be prime candidates for molecular activation and catalysis in the solid-state.⁵

Unfortunately, the direct incorporation of low-valent 4d and 5d metals into MOFs as the primary inorganic structural elements is generally difficult to achieve.⁶ Low-valent metal ions tend to favor coordination to soft ligand donors (e.g., phosphines, carbonyls) and are less compatible with harder ligand donors commonly utilized in MOF chemistry (e.g., carboxylates and azolates).⁷ Softer, covalent metal–ligand bonds are also more rapidly hydrolyzed than hard–hard electrostatic bonds between 3d metal ions and hard ligand anions. Furthermore, low-valent metal precursors are susceptible to oxidation under common MOF-forming reaction conditions.

One effective and increasingly popular synthetic strategy used to circumvent these intractable issues involves the preparation of MOFs using ligands with both hard (i.e., charged anionic) and softer (i.e., Lewis base) donor groups.⁸ Treatment of such ligands with common MOF-forming metals in aqueous–organic solvent mixtures can achieve the crystallization of new MOFs, which are decorated with accessible Lewis base sites suitable for postsynthetic coordination with secondary low-valent metal species. Yaghi,⁹ Cohen,¹⁰ Doonan & Sumbly¹¹ and others originally demonstrated the functionalization of MOFs containing pendant Lewis base moieties, such as pyridines,^{9a,10a} alkoxides,^{10b} and carbenes.^{9b,11}

Given the ubiquitous nature of organophosphines (R₃P) in molecular coordination complexes of a wide range of low-valent metals, we have focused on the discovery of a continually expanding family of MOFs decorated with periodic soft P(III) donors,¹² referred to as phosphine coordination

Received: May 30, 2021

Published: August 19, 2021



materials (PCMs). PCMs based on poly(carboxylated) triarylphosphine building blocks exhibit accessible internal surface areas and stabilities that are comparable to other MOFs, but are uniquely able to coordinate a variety of low-valent metals by simple ligand displacement reactions under facile reaction conditions.¹² An analogous strategy has also more recently been applied to the synthesis of arsine (R₃As)-based MOFs.¹³

PCMs can be alternatively derived using preformed metal-phosphine coordination complexes as “metalloligand” building blocks (e.g., BINAP,¹⁴ bis(phosphine)¹⁵, or pincer¹⁶ complexes), but their syntheses are often arduous and are not amenable to scale. In comparison, triphenylphosphine-based ligands adapted for MOF synthesis, such as, tris(*p*-carboxylato)triphenylphosphine (tctpH₃; P(C₆H₄-4-CO₂H)₃),¹⁷ can be prepared in only two steps and on a multigram scale. We recently reported the MOF PCM-101, which contains periodic *trans*-P₂ pockets having a P...P separation of 7.2 Å. In essence, PCM-101 is an infinite “solid-state ligand” (SSL), which provides rigid coordination pockets that are otherwise difficult to access using molecular bidentate bis(phosphine) ligands.^{12a} Perhaps most notably, this MOF was obtained by leveraging core reticular chemistry concepts,¹ whereby a judicious choice of inorganic nodes and secondary pillaring ligands (i.e., 4,4'-bipyridine) enabled the directed assembly of monophosphines in the solid-state, to generate cooperative *trans*-P₂ pockets. The as-synthesized PCM-101 underwent postsynthetic metalation with different low-valent metals, and the structural changes were observed by single-crystal X-ray diffraction (SCXRD). Direct metalation of the P₂ pockets by treatment with (Me₂S)CuBr at room temperature achieved the installation of phosphine-capped Cu₂Br₂ dimers. The resulting material displayed significantly enhanced N₂ adsorption and decreased CO₂ adsorption relative to the unmetalated parent material as well as unexpected catalytic capabilities when exposed to alkynols.^{12a}

RESULTS AND DISCUSSION

Synthesis and Structure of PCM-102. Based on this exciting result, we have continued to search for other new network topologies using the same tctpH₃ ligand. The original reaction conditions used to obtain PCM-101 were modified by adding excess benzoic acid to a solution of tctpH₃, 4,4'-bipyridine, and Co(BF₄)₂ in a 5:2:1 (v/v) DMF/MeOH/H₂O mixture. Benzoic acid was added to regulate the rate of ligand deprotonation; it is also able to play a role in modulating the rate of 4,4'-bipy incorporation into pillared MOFs via the formation of putative pyridinium benzoate species, based on comparative pK_a values (PhCO₂H = 4.2; bipyH⁺ ~ 5).¹⁸ After heating at 100 °C for 24 h, a single phase consisting of large red prismatic crystals was obtained, distinct in morphology and color compared with PCM-101.

SCXRD revealed that a new MOF structure had been realized, based on the repeat unit [(H₃C)₂NH₂][Co₃(μ₃-OH_{0.44}F_{0.56})(tctp)₂(4,4'-bipy)(OH₂)]·*solv.*, hereafter referred to as, PCM-102. The new MOF crystallizes in the monoclinic space group *P2₁/n* (*Z* = 4). PCM-102 is a three-dimensional network based on the coordination of tctp³⁻ and 4,4'-bipy ligands to triangular [Co₃(μ₃-OH/F)]⁵⁺ metal nodes (Figure 1A). As seen in Figure 1A, the symmetrically inequivalent Co1, Co2, and Co3 atoms are octahedrally coordinated. The central μ₃-bridging atom in each Co₃ trimer is either OH⁻ or F⁻ with an overall OH:F ratio of 1:1.27, determined by elemental

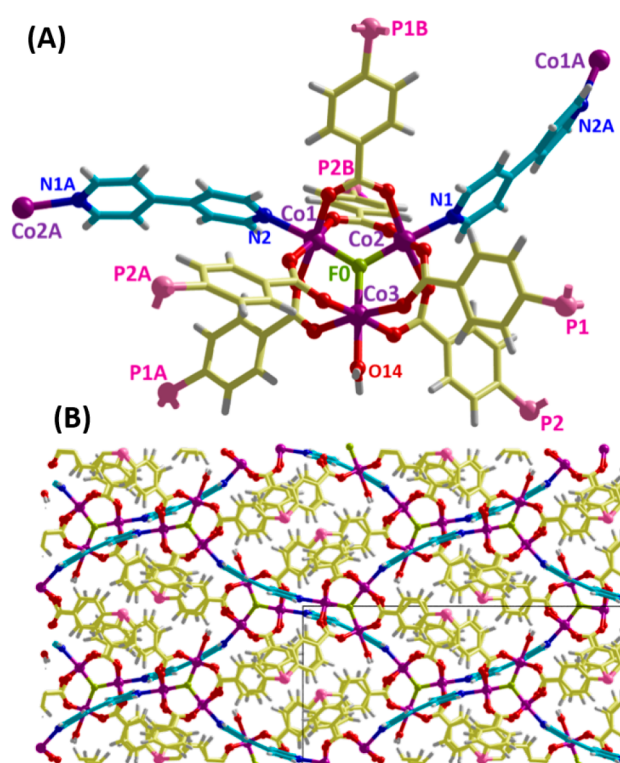


Figure 1. (A) An 8-connected [Co₃(μ₃-F)]⁵⁺ node in PCM-102 showing coordination by six tctp³⁻ ligands and two 4,4'-bipy ligands (bipy C atoms are drawn in cyan for clarity). (B) Extended packing view of PCM-102 in the *ab*-plane, showing pairs of offset phosphines within the close-packed network.

microanalysis and associated characterizing data. In this case, F⁻ is presumably derived by the partial hydrolysis of BF₄⁻ counterions. The absence of μ₃-O²⁻ was confirmed by bond-valence sum (BVS) calculations using SCXRD-derived atomic distances (Table S1). Accordingly, all metals in the [Co₃(μ₃-OH/F)]⁵⁺ nodes are Co(II); coordination by six *syn*,*syn*-bridged carboxylate groups results in a pseudo-octahedral arrangement of P(III) sites around each node (Figure 1A). Two of the three Co(II) axial sites are coordinated by 4,4'-bipy-*N* atoms that bridge to neighboring nodes (Figure 1A, cyan), while the third axial site is coordinated by a terminal OH₂ ligand (Figure 1A, O14).

Importantly, the PCM-102 network is monoanionic per repeat unit, and charge-balance is achieved by the presence of one dimethylammonium (Me₂NH₂⁺) counterion per repeat unit, which was directly located within the micropores from the single crystal data. Elemental and thermogravimetric analyses (TGA) further confirmed the identity of the cation (see Experimental Section and Figure S1).

PCM-102 is an 8,3-connected MOF, in which pairs of phosphine-*P* atoms are arranged in an offset *trans* orientation (Figure 1B; pink atoms). Each pair of offset P(III) atoms are related by an inversion center, such that the lone pairs project at 180° with respect to one another; the P...P separation distance within each offset pair is 3.64 Å and the lateral offset is ~2.8 Å. The aryl C–P–C angles within the two symmetrically unique tctp³⁻ ligands lie in the range 100.1–101.9°, indicating the presence of a P(III) lone pair of electrons.¹⁹ ³¹P magic-angle spinning (MAS)-NMR studies of PCM-102 identified a single peak at 5.38 ppm, confirming the presence of P(III) sites that had not become oxidized during the synthesis or upon

exposure of the crystalline solid to the air (Figure S2). A view of PCM-102 in the crystallographic *ab*-plane (Figure 1B) suggests that PCM-102 is nonporous; however, small rhombic pores with guest-accessible dimensions of ca. $6.7 \times 8.2 \text{ \AA}$ (estimated from interatomic distances and considering van der Waals radii) are observed when viewed parallel to the *a*-axis (Figure S3). These apertures are large enough to provide access of adsorbed substrates to the vacant P(III) sites within the PCM-102 structure.

PCM-102 was easily prepared on larger (gram) scales using the original method, and phase purity was confirmed by powder X-ray diffraction (PXRD), based on close agreement between experimental data and the expected pattern simulated from the SCXRD data (Figure 2, black data). TGA studies of

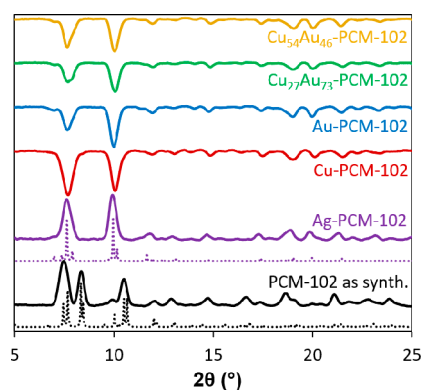


Figure 2. Bottom: Comparison of PXRD patterns for the parent PCM-102 (black) with the Ag(I)-pillared derivative (purple) versus the respective simulated patterns (dashed lines). Top: PXRD patterns for PCM-102 analogues with other pillaring metals, confirming network isostructurality.

PCM-102 displayed a mass loss of $\sim 22\%$ between room temperature and $140 \text{ }^\circ\text{C}$, which was attributed to the loss of pore-based solvent molecules (Figure S1). Upon continued heating, the material remained stable up to $360 \text{ }^\circ\text{C}$, beyond which the onset of thermal decomposition was observed.

A sample of as-synthesized PCM-102 was desolvated by heating at $75 \text{ }^\circ\text{C}$ under high vacuum, and various gas sorption isotherms were collected using different small molecule probe gases (N_2 , CO_2 , O_2 , CH_4 , H_2). For all gases, PCM-102 displayed negligible or low uptakes in the range 0–1 atm, with estimated Brunauer–Emmett–Teller (BET) surface areas of ~ 0 and $110 \text{ m}^2 \text{ g}^{-1}$ for N_2 and CO_2 , respectively (Figure S4). The low accessible surface area of PCM-102 was attributed to the small pore apertures and potential collapse of the pore structure upon desolvation, which has been seen previously for similar materials.²⁰

Ag(I) Pillaring Studies of PCM-102. Since Ag(I) is known to form complexes of the type, $[\text{Ag}(\text{PPh}_3)_2(\text{NO}_3)]$,²¹ as well as related cationic complexes, $[\text{Ag}(\text{PPh}_3)_2\text{L}]^+$ (where L is a neutral 2-electron donor ligand),²² we hoped to install similar complexes between the offset phosphine pairs in PCM-102. We therefore attempted syntheses in which 0.5 equiv of AgNO_3 (with respect to tctpH_3) was added to the reaction mixture. Care was taken to exclude atmospheric oxygen and visible light from the reaction vials to prevent Ag reduction. Large red prismatic crystals of a new material were obtained under similar reaction conditions after heating at $75 \text{ }^\circ\text{C}$, with no benzoic modulator needed in this case. Several distinct

differences were observed in the PXRD pattern of the new material (Figure 2, purple data). To our pleasant surprise, SCXRD analysis revealed the successful insertion of Ag(I) sites between adjacent P donors, but in a near-linear orientation and without any other species closely associated with the Ag center (Figure 3). The network connectivity of Ag-PCM-102 is otherwise identical to the parent PCM-102, but Ag-PCM-102 crystallizes into the higher-symmetry *Pnma* orthorhombic setting.

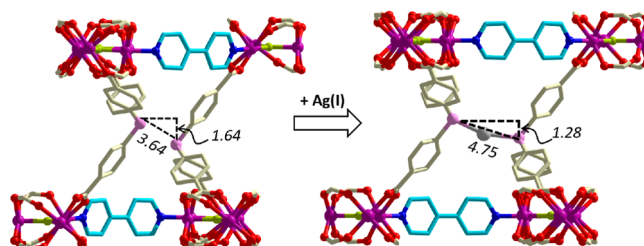


Figure 3. SCXRD structural comparison between the parent PCM-102 and upon installation of Ag(I) pillars by linear coordination with adjacent phosphines; distances are shown in Å.

Ag-PCM-102 is a heterobimetallic MOF, in which Ag(I) ions act as additional linear, 2-connected pillars that force *trans*-alignment of the originally staggered P_2 (bis(phosphine)) moieties (Figure 3). This process can be considered analogous to regular MOF pillaring strategies with organic linkers such as 4,4'-bipy, except that in this unique case, the pillar is the Lewis acid and the MOF is the Lewis base. In this case, the Ag(I) pillars do not serve to add dimensionality to the structure (since PCM-102 is a three-dimensional MOF to begin with), but act as additional, linear and rigid supports to increase the overall network connectivity. Furthermore, it was found that Ag(I) ions had directly substituted the uncoordinated $[\text{Me}_2\text{NH}_2]^+$ ions (Experimental Section and Supporting Information), resulting in a counterion-free, charge-neutral MOF with formula, $[\text{Co}_3(\mu_3\text{-OH}_{0.44}\text{F}_{0.56})\text{Ag}(\text{tctp})_2(4,4'\text{-bipy})\text{-}(\text{OH}_2)]$. The site occupancy of Ag in the SCXRD was freely refined to 100%. Inductively coupled plasma-optical emission spectroscopy (ICP-OES) of the bulk sample provided an Ag loading of 102.6%, also confirming complete installation of Ag(I) pillars (Table S2). Furthermore, PXRD, transmission electron microscopy (TEM), scanning electron microscopy (SEM), and X-ray photoelectron spectroscopy (XPS) studies confirmed the absence of any structures that could be attributed to Ag(0) (Figures S5–S8).

This is a highly noteworthy result, since it demonstrates a novel and potentially powerful principle for the isolation of counterion-free low-valent metal species using the MOF itself as the counterion. Taken more generally, this approach could provide access to other catalyst species whose activities are not dependent upon the use of weakly coordinating anions, as they are in the classical, homogeneous setting.²³

The extent of the structural distortions induced by Ag-pillaring of the original PCM-102 network are shown in Figure 3, which reveals a significant opening of the pores. When considered geometrically, the cross-pore P...P distance was increased by 1.1 \AA and opposing phosphines also shifted laterally by 0.36 \AA to permit *trans*-chelation of Ag(I). The resulting *trans*- $[\text{P}_2\text{Ag}]^+$ pillars have a P–Ag–P angle of 159.1° ; the corresponding P–Ag distances (2.36 and 2.47 \AA) are within the range observed for molecular P(III)–Ag(I) bonds

(Table S3).²⁴ When Ag-PCM-102 was subjected to gas adsorption analysis, its estimated CO₂ BET surface area was found to be 1558 m² g⁻¹ (cf. PCM-102; S_{CO₂}^{BET} = 110 m² g⁻¹; Figure 4A, black vs purple data). Furthermore, Ag-PCM-102

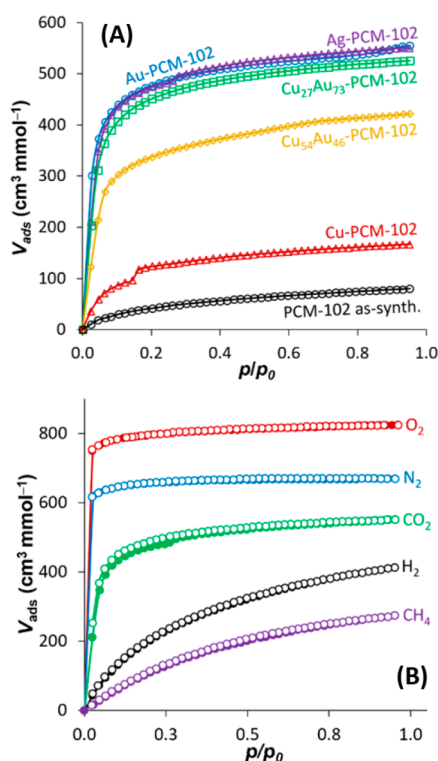


Figure 4. (A) Comparison of CO₂ adsorption isotherms (196 K) for the parent PCM-102 and various metal-pillared analogues. (B) Comparison of sorption isotherms in Ag-PCM-102 using different probe gases: O₂, N₂, H₂ (77 K); CO₂, CH₄ (196 K); solid circles = adsorption, open circles = desorption.

showed appreciable uptakes of CH₄, H₂, N₂, and O₂ (273, 413, 670, and 824 cm³ mmol⁻¹, respectively), with an estimated S_{N₂}^{BET} = 1550 m² g⁻¹ (Figure 4B). Here, we employ units of cm³ mmol⁻¹ for comparison purposes, because addition of Ag(I) pillaring ions significantly increases the molar mass of the MOF.

Clearly, the installation of *trans*-[P₂Ag]⁺ pillars in PCM-102 had significantly increased its permanent microporosity. Perhaps more surprising was the subsequent discovery that Ag-PCM-102 could also be cleanly obtained via direct postsynthetic metalation of as-synthesized and air-dried PCM-102 crystals. This was achieved by simple immersion of crystals in a solution containing 0.55 equiv of AgNO₃ (per tctp³⁻) dissolved in 5:2:1 (v/v) DMF/MeOH/H₂O, which was left to stand in the dark at room temperature for 18 h. After isolating the crystals and washing with fresh solvent, PXRD confirmed that PCM-102 had undergone a transformation to yield the Ag-PCM-102 pillared material (Figure S9). This is an example of “soft crystal” behavior,²⁵ in that the preformed PCM-102 permitted a significant periodic distortion in order to accommodate Ag(I) ions between the initially staggered bis(phosphine) pockets. To the best of our knowledge, this is the first example in which a MOF constructed using monodentate phosphine ligands has been used for postsynthetic chelation of a single metal center,

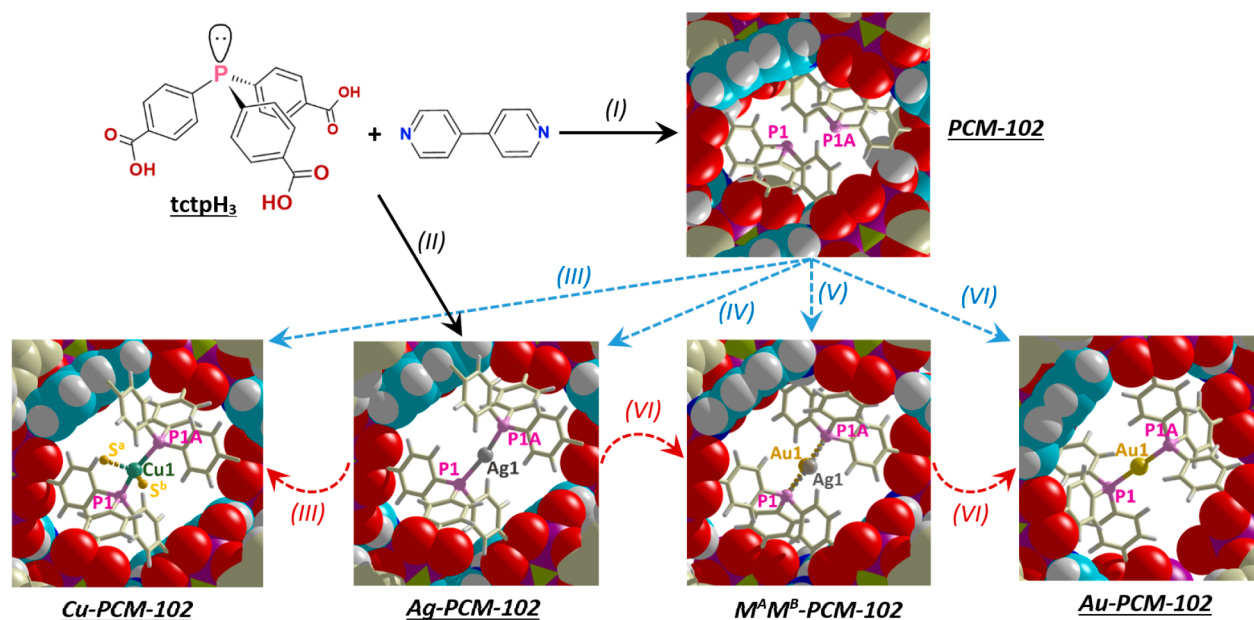
analogous to the “molecular trapping” approach that has been demonstrated for CO₂.²⁶ Unlike traditional molecular bis-(phosphine) ligands that favor the formation of cisoid chelates, PCM-102 enables the use of simple monophosphines to construct more unusual *trans*-chelators.

Broad Scope Pillaring of PCM-102 with Cu(I), Au(I), and Mixed-Metal Pillars. To further explore the potential scope of metal pillaring in PCM-102, we next studied the potential postsynthetic modification of PCM-102 with other group 11 ions. Treatment of PCM-102 with solutions containing (Me₂S)CuBr and (Me₂S)AuCl resulted in products with PXRD patterns that closely matched that of Ag-PCM-102 (Figure 2, red and blue data). Fortunately, crystals suitable for SCXRD analysis were directly obtained from both the Cu(I)- and Au(I)-treated samples (Figures S10 and S11). The resulting SCXRD solutions confirmed successful metalation in both cases. Scheme 1 compares the crystal structures of a single [P₂M]⁺ pillar (M = Cu, Ag, Au) in each M-PCM-102 analogue and illustrates how each material was synthetically derived in this study.

As shown in Scheme 1, Cu(I) ions adopt a 4-coordinate distorted seesaw structure, with a P–Cu–P bond angle of 147.5°. Each Cu(I) is coordinated by two solvent oxygen atoms (Scheme 1, S^a and S^b; each has 1/2 site occupancy) that belong to coordinated DMF molecules (Figure S12). The Cu(I) centers do not sit equidistant from both phosphine sites, having crystallographically distinct P–Cu distances of 2.17 and 2.33 Å. The P–Cu bond distances and P–Cu–P bond angle are both outside the range determined for analogous molecular complexes in the CCDC (Table S3).²⁷ This implies that geometric strain is imparted in this complex, such that the MOF truly acts as a rigid SSL, which cannot adopt an equilibrium coordination environment around the Cu(I) as it would in the molecular setting (Table 1). In stark contrast, Au(I) ions were found to adopt a perfectly linear P–Au–P coordination mode with P–Au distances of 2.30 Å, which are within the range observed for molecular complexes (Table S3).²⁸ The overall trend in coordination geometries observed in the Cu–Ag–Au series follows the increasing ionic radii of the M(I) ions as well as the increasing softness of the metal, resulting in the formation of increasingly more stable coordination bonds.

Interestingly, while Ag-PCM-102 could be obtained both *peri*- and postsynthetically (Scheme 1, (ii) and (iv)), the Cu- and Au-PCM-102 analogues could only be cleanly obtained via postsynthetic treatment of PCM-102 (Scheme 1, (iii) and (vi)). It is reasonable to assume that AgNO₃ provides “naked” Ag(I) ions that are likely to form [Ag(tctpH₃)₂]⁺ secondary building units in solution. The same mechanism may not be feasible for (Me₂S)CuBr or (Me₂S)AuCl: Although dimethylsulfide is a weakly bound ligand that is readily displaced in coordinating solvents, the metal–halide bonds are somewhat stronger and are likely to form neutral [(tctpH₃)(L)CuBr]₂ (L = neutral ligand or coordinating solvent) or (tctpH₃)AuCl precursor complexes in solution.²⁹ These putative complexes would impede the direct formation of M-PCM-102. It is also possible that Cu(I) or Au(I) ions preferentially coordinate to 4,4'-bipy in solution, which would similarly deter crystallization of the target pillared PCM-102 phases.

The site occupancies of postsynthetically installed Cu(I) and Au(I) pillars were unity from the crystal structure data; accordingly, digested samples were studied by ICP-OES and yielded experimental loadings of 142 and 91%, respectively

Scheme 1. Feasible Synthetic Routes toward PCM-102 and the Metal-Pillared M-PCM-102 Derivatives^a

^aSolid black arrows represent direct reactions; dashed blue arrows represent post-synthetic metallations; dashed red arrows represent metal pillar interchange by post-synthetic exchange. Reaction conditions: (i) = 16 equiv PhCO₂H, 3 equiv Co(BF₄)₂, 100 °C, 24 h; (ii) = 0.5 equiv AgNO₃, 3 equiv Co(BF₄)₂, 75 °C, 24 h; (iii) = 1.5–2.0 equiv (Me₂S)CuBr; (iv) = 0.5 equiv AgNO₃; (v) = sequential addition of 0.6 equiv M^A and 0.6 equiv M^B; (vi) = 0.5–1.5 equiv (Me₂S)AuCl. All reactions performed in 5:2:1 DMF/MeOH/H₂O.

Table 1. DFT Binding Energies for C2 Hydrocarbons in Ag-PCM-102

system	binding energy (eV)	binding energy without vdW (eV)	estimated vdW interaction (eV)
MOF-C ₂ H ₆	−0.24	0.05	0.29
MOF-C ₂ H ₄	−0.11	0.14	0.25
MOF-C ₂ H ₂	−0.29	−0.12	0.17

(Tables S4 and S5). Complete functionalization of a given MOF by postsynthetic treatment is usually exceedingly difficult to achieve;^{11b,c} this indicates that chelation by PCM-102 is thermodynamically favorable, allowing all metallations to proceed to near-completion. In the case of Cu-PCM-102, a 2-fold excess of the Cu(I) precursor was needed to achieve full conversion, and the excess Cu determined by ICP-OES was attributed to an unidentified Cu(I) impurity which was insoluble and could not be removed by washing. XPS analyses of all M-PCM-102 materials indicated that the pillaring metal remained in the +1 oxidation state. For Au-PCM-102, a small proportion of Au(0) (8%) was detected (Figures S13 and S14).

Perhaps the most remarkable synthetic discovery made in this work was that the preformed Ag-PCM-102 could be used as a sacrificial precursor for the formation of Cu-, Au-, and mixed-metal Ag/M-PCM-102 materials, via postsynthetic metal exchange reactions.³⁰ As shown in Scheme 1 (red dashed arrows), when Ag-PCM-102 was exposed to controlled amounts of (Me₂S)CuBr or (Me₂S)AuCl, Ag was preferentially displaced, resulting in materials that retained full crystallinity and were characterized by SCXRD. The expected driving force for this interesting reaction was the precipitation of AgCl or AgBr, which were detected in the resulting PXRD patterns

(Figure S15). The AgX byproducts were effectively removed by rinsing the crystalline solids with dilute NH₄OH (0.1 M in 5:2:1 DMF/MeOH/H₂O), with no loss of crystallinity observed by PXRD (Figure S15). While the metal interchange process employed to obtain Cu-, Au-, or mixed-metal PCM-102 derivatives proceeded smoothly using Ag-PCM-102 as the starting material, the reverse process (i.e., using Au-PCM-102 and treating with Ag(I) ions) only resulted in low pillar substitution (ca. 8% by ICP-OES analysis). Furthermore, PXRD analysis of exchange reactions employing Cu-PCM-102 as the precursor indicated the coformation of some Ag(0) species. We therefore surmise that the thermodynamic driving force to precipitate AgX salts is crucial in this process.

Under the metal exchange approach, Ag(I) pillars could be completely replaced by Cu(I) or Au(I) if exposed to a slight molar excess of the pillaring precursors. Perhaps most interestingly, when substoichiometric amounts of Cu(I) or Au(I) precursors were employed, we were able to make bimetallic M^AM^B-PCM-102 analogues with M^A:M^B ratios dictated by the precursor ratios employed (Figure S16). To fully complete the synthetic roadmap outlined in Scheme 1, Cu/Au-PCM-102 bimetallic materials could also be obtained by sequential addition of substoichiometric amounts of Cu(I) and Au(I) precursors.

The gas sorption properties of the Cu- and Au-PCM-102 materials were determined using the same probe gases and conditions as employed above (Figures S17 and S18). Compared with PCM-102, the pillared materials displayed significantly enhanced gas uptakes (Figure 4A). The estimated CO₂ BET surface areas for Cu- and Au-PCM-102 were 434 and 1449 m² g^{−1}, respectively (cf. Ag-PCM-102, S_{BET}^{CO₂} = 1558 m² g^{−1}). Both Cu- and Au-PCM-102 also showed similar internal surface areas using N₂ as the adsorbate.

The comparatively low uptake of Cu-PCM-102 compared to the Ag(I) and Au(I) derivatives (Figure 4A) was assumed to

be due to the bent coordination geometry of the $[P_2Cu(DMF)]^+$ moieties and the contracted nature of Cu(I) valence orbitals, resulting in more labile P–Cu bonds enabling structural collapse upon activation. To explore this premise further, we attempted to see if incorporation of some Au(I) pillars in addition to Cu(I) pillars could stabilize the material, while still employing a significant proportion of economically more attractive Cu(I) ions.

To do so, a partially metalated sample of Cu-PCM-102 was exposed to a substoichiometric amount of the Au precursor and then isolated for characterization (Figure S19). The total metal loading of CuAu-PCM-102 was determined to be 100.1% by ICP-OES (Cu + Au), and the ratio of Cu:Au was 0.42, or $Cu_{29}Au_{71}$ -PCM-102 (Table S6). A material with the formula $Cu_{57}Au_{43}$ was similarly obtained by partial metalation with Au(I) followed by treatment with Cu(I). $Cu_{29}Au_{71}$ -PCM-102 gave N_2 and CO_2 BET surface areas of 1435 and $1451\text{ m}^2\text{ g}^{-1}$, respectively (Figure 4A), which are comparable to the values obtained for monometallic Au-PCM-102 (1511 and $1449\text{ m}^2\text{ g}^{-1}$). These data suggest that adding a proportion of more stable Au pillars alongside Cu pillars is indeed an effective strategy to infer long-range stability into the PCM-102 materials.

Selective C2 Adsorption by the M-PCM-102 Materials. Evidently, *trans* chelation of secondary metals by the P_2 sites increased the sorption capacities of the materials, with stronger P–M bonds ($M = Ag(I), Au(I)$) resulting in materials with greater stability and higher gas uptakes than those with weaker P–M bonds ($M = Cu(I)$). Dissociated $LM^+\cdots X^-$ species are known to facilitate moderately strong interactions between low coordinate M(I) sites and unsaturated hydrocarbons via σ -donor interactions between valence metal orbitals and hydrocarbon π -bonds. These interactions have been exploited in some large-scale hydrocarbon separations to improve adsorption affinity (i.e., retention) of unsaturated C=C bonds over saturated alkanes (e.g., aqueous $AgNO_3$ solutions).³¹ Meanwhile, linear P_2M^+ species, such as those present in the M-PCM-102 MOFs, are likely to be less Lewis acidic due to the presence of a secondary phosphine donor; phosphine dissociation in the MOF is also inhibited, thus limiting access to singly coordinate $L-M^+$ species. However, unlike in the molecular setting, access to the M^+ sites is uninhibited due to the absence of weakly coordinating anions.

Based on the above, we decided to evaluate the metalated PCM-102 materials for the separation of C2 hydrocarbons, to probe the extent to which the identity of the metal could engender desirable adsorption selectivity. As a first step, sorption isotherms were collected at $30\text{ }^\circ\text{C}$ for Cu-, Ag-, and Au-PCM-102 as well as mixed-metal $Cu_{29}Au_{71}$ -PCM-102, using ethane (C_2H_6), ethylene (C_2H_4), and acetylene (C_2H_2) as probe gases (Figure 5, Figure S20). Some unexpected trends were observed in the C2 sorption data that were clearly dependent on the metal(s) incorporated. When considering pure physisorption interactions between the host MOF and guest adsorbate, the expected trend in affinity should follow increasing polarizability of the probe gas, which induces a greater number of host–guest dipole–dipole interactions. The expected adsorption affinity series would thus be $C_2H_6 > C_2H_4 > C_2H_2$. Conversely, when considering direct (orbital–orbital) interactions between the M(I) sites and guest hydrocarbons, the order of adsorption affinity should be reversed ($C_2H_6 < C_2H_4 < C_2H_2$), since $C\equiv C$ bonds are stronger σ -donors than $C=C$ bonds.

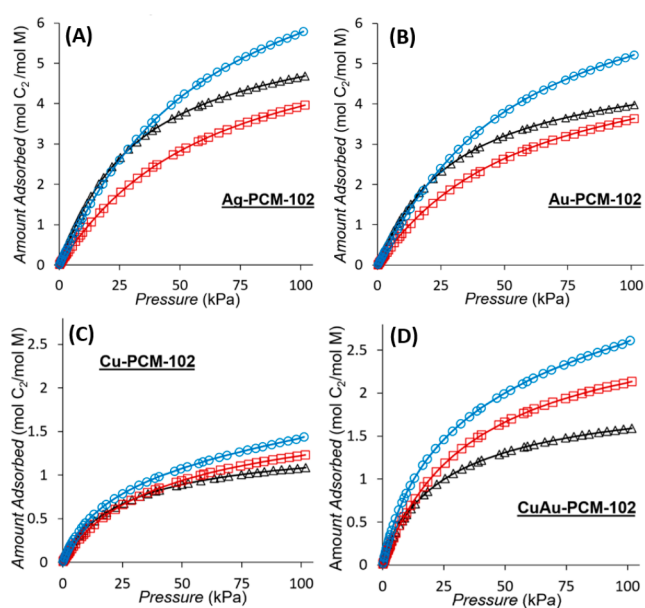


Figure 5. Comparison of C2 gas adsorption isotherms in the M-PCM-102 materials: C_2H_2 (blue circles), C_2H_4 (red squares), and C_2H_6 (black triangles).

The sorption capacities observed for the M-PCM-102 materials are similar to other benchmark MOFs that have been studied for this application.³² Surprisingly, the observed trends in sorption selectivity for Ag- and Au-PCM-102 deviate from both of the above-mentioned predictions, having sorption capacities of the order, $C_2H_2 > C_2H_6 > C_2H_4$ (Figure 5A,B). In contrast, the Cu-pillared analogue displayed a more common trend in selectivity of the order $C_2H_6 < C_2H_4 < C_2H_2$ (Figure 5C), albeit with significantly lower overall capacities at 100 kPa (~ 24 – 28% cf. Ag-PCM-102), which is in line with the lower estimated surface area of this material. Interestingly, the bimetallic $Cu_{29}Au_{71}$ analogue enabled higher overall sorption capacities (intermediate between the pure Cu- and Au-pillared materials), but the relative order of capacities was the same as for Cu-PCM-102 (Figure 5D).

Taken together, these interesting results suggest that the apparent ordering of sorption capacities for the different analogues is due to competing host–guest interactions, in which physisorption interactions with the pore surfaces as well as the identity of the pillaring metal both play significant roles. The affinity for ethane over ethylene was not anticipated, but has been reported previously for materials in which ethane protons interact favorably with aromatic rings present within porous materials.³³ Cu-PCM-102 gives the selectivity predicted by considering only metal–hydrocarbon interactions, although with low overall sorption capacities. In this case, the partial collapse of the pore structure hinders access to the internal structure. Interestingly, CuAu-PCM-102 displays the same C2 adsorption trend as the pure Cu material, despite the relatively high proportion of Au in the material (mol Au/mol Cu = 2.4). The sorption capacities for both Cu-containing materials were in the order $C_2H_2 > C_2H_4 > C_2H_6$, while CuAu-PCM-102 gave a higher overall uptake and displayed larger ratios in the quantities adsorbed. This demonstrates that the mixed-metal approach can be used to realize a system in which the selectivity imparted by Cu(I) is enhanced relative to the pure Cu system, despite the different selectivity observed for the pure Au material. The higher affinity for unsaturated

hydrocarbons over ethane in the Cu(I)-containing systems is consistent with the stronger Lewis acidity of Cu(I) compared to Ag(I) and Au(I). In this case, $\text{Cu}\cdots\pi$ interactions dominate over physisorption interactions. These results describe the unique opportunity presented by the M-PCM-102 family of materials: The affinity of the materials for different adsorbates can be systematically tuned by changing the identity of M, with further tunability likely possible using different multimetallic systems.

From the sorption isotherms, we determined that the most viable separation would be the separation of ethylene and acetylene using Ag-PCM-102. Sorption isotherms were collected for Ag-PCM-102 at 10, 20, and 30 °C using ethylene and acetylene probe gases. Ideal adsorbed solution theory (IAST)³⁴ was used to determine the selectivity for acetylene, which was calculated as 1.5 at 1 bar and 303 K for both 50:50 and 99:1 ratios of ethylene/acetylene (Figure 6). The

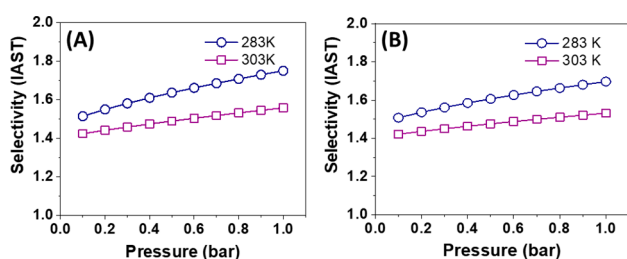


Figure 6. IAST selectivity for acetylene over ethylene for Ag-PCM-102 at 283 K (blue circles) and 303 K (purple squares) with an ethylene/acetylene ratio of (A) 50:50 and (B) 99:1.

experimental isosteric heat of adsorption (Q_{st}) values were calculated from the data using a dual-site Langmuir model, which gave values of 20 kJ mol^{-1} for ethylene and 27 kJ mol^{-1} for acetylene at zero coverage (Figure 6).

DFT Analysis of C2 Hydrocarbon Sorption Behavior.

To understand the experimental adsorption profiles of the C2 hydrocarbons in Ag-PCM-102, density functional theory (DFT) calculations were performed to model the binding energies for the adsorption of C_2H_6 , C_2H_4 , and C_2H_2 . The calculated binding energies for the three C2 hydrocarbons in Ag-PCM-102 are shown in Table 1. Calculations show that acetylene (C_2H_2) binds most strongly within the MOF, while ethylene (C_2H_4) binds the weakest, in direct agreement with the experimental data (Figure 5A). The strength of van der Waals (vdW) interactions between the C2 molecules and the MOF structure was estimated by calculating the binding energies with and without vdW forces considered, followed by subtraction of the two values (Table 1).

The presence of π -bonds in unsaturated C_2H_4 and C_2H_2 was expected to increase binding to the metal center, yet surprisingly C_2H_4 was bound most weakly among the three molecules. The Ag(I) sites have an open-shell ($4d^9 5s^1$) configuration, based on the calculated spin state. To investigate potential interactions between the metal center and the C2 molecules, the Bader charges on the Ag and P sites belonging to a single $[\text{Ag}(\text{tctp})_2]^+$ unit were calculated (Table S7). The charges on the Ag and P sites were not found to change significantly upon molecular adsorption, which indicates minimal interaction between the metal center and all three C2 hydrocarbons. This result is consistent with the distances between the metal centers and the adsorbed C2 molecules (>3.7 Å). In fact, the strongest interactions between the C2

molecules and the MOF occur at the phenyl rings, which can be seen by considering the frontier orbitals of the C2 molecules and the Ag(I) sites (Figure 7). There is no apparent

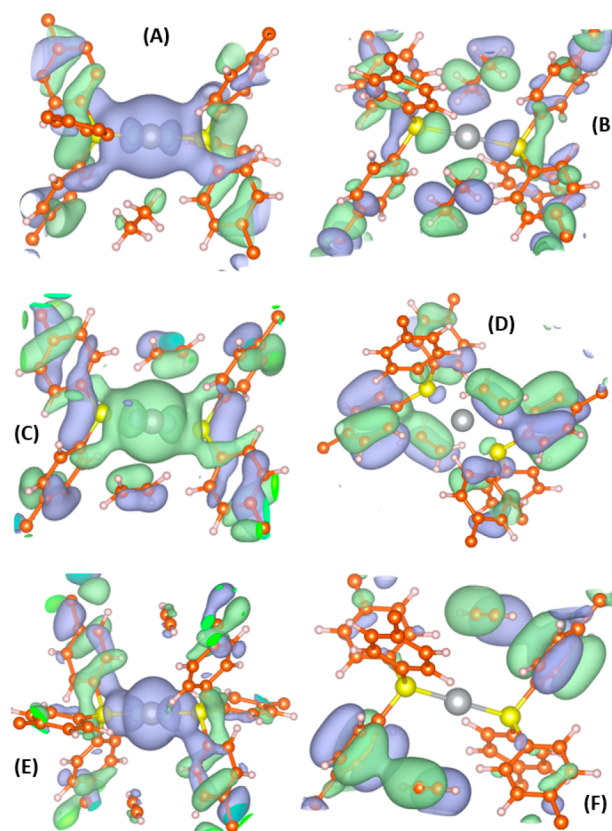


Figure 7. Plots of orbitals on the metal center (left column) and the phenyl rings (right column) for Ag-PCM-102 loaded with (A, B) C_2H_6 , (C, D) C_2H_4 , and (E, F) C_2H_2 . Color scheme: C, orange; P, yellow; Ag, gray; H, white.

overlap between the highest energy orbitals on the Ag center and the C2 molecules (Figure 7A,C,E), and no orbital overlap is observed between C_2H_6 and the nearest MOF phenyl ring (Figure 7B). However, there is detectable orbital overlap between the C2 adsorbates and the phenyl ring in the case of both C_2H_4 (Figure 7D) and C_2H_2 (Figure 7F).

To understand the unusual observed binding trend of C2 hydrocarbons in Ag-PCM-102 ($\text{C}_2\text{H}_2 > \text{C}_2\text{H}_6 > \text{C}_2\text{H}_4$), two different binding interactions must be considered in concert. First, Table 1 shows that vdW interactions systematically increase with hydrocarbon saturation, as expected. This explains the fact that saturated C_2H_6 binds more strongly than C_2H_4 , but not why C_2H_2 has the strongest binding. The second factor that explains the strong acetylene binding is the strong C–H bond dipoles present in C_2H_2 , which induce favorable electrostatic interactions with C atoms of the phenyl rings. Table 2 shows the Bader charges on C and H in the C2

Table 2. Bader Charge of the Carbon and Hydrogen Atoms for C2 Molecules in the Gas Phase and Bound in the MOF

Bader charge	C_2H_6	MOF- C_2H_6	C_2H_4	MOF- C_2H_4	C_2H_2	MOF- C_2H_2
C	0.08	−0.10	−0.19	−0.14	−0.39	−0.43
H	−0.08	0.09	0.09	0.15	0.39	0.43

molecules, both free and loaded in the MOF. It is apparent from these values that C_2H_2 has a much stronger C–H dipole compared to C_2H_4 and C_2H_6 . These dipole–phenyl ring interactions can be understood visually in Figure 8, with a view

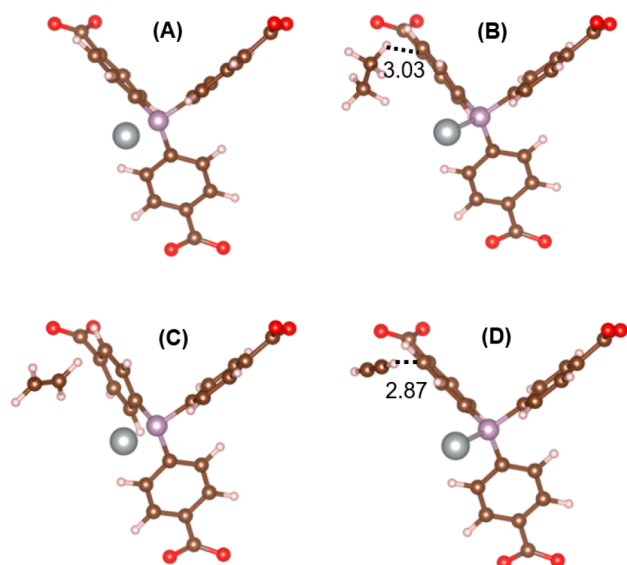


Figure 8. (A) View of a single phosphine ligand in Ag-PCM-102 and (B–D) are corresponding views when bound to C_2H_6 , C_2H_4 , and C_2H_2 , respectively. Color scheme: C, brown; P, purple; Ag, gray; O, red; H, white. Contact distances are shown in Å.

of guest-free Ag-PCM-102 shown for reference (Figure 8A). Here, it can be seen that C_2H_6 binding is nonspecific and the closest distance between any H atom on C_2H_6 and a C atom on the nearest phenyl ring is 3.03 Å (Figure 8B). A similarly nonspecific interaction is observed for C_2H_4 (Figure 8C). In contrast, the more polarized C–H bonds of C_2H_2 point directly toward C atoms on the phenyl ring (Figure 8D) at a significantly shorter distance of 2.87 Å.

These DFT studies agree well the experimental C_2 sorption data and elucidate the nature of the interactions between the various C_2 molecules and PCM-102. The calculations suggest that C_2H_2 binds to the aromatic regions of the MOF pore walls due to the strong dipolar coupling, which results in significant wave function overlap with the MOF phenyl rings. C_2H_6 binds strongly via a nonspecific vdW interaction, while C_2H_4 binds most weakly as it displays only modest vdW interactions and weaker dipole–aryl interactions.

CONCLUSIONS

In summary, a unique MOF containing offset P_2 pockets, PCM-102, was found to act as a flexible solid-state ligand. Postsynthetic chelation of Cu(I), Ag(I), and Au(I) was achieved with high degrees of metal incorporation, and the metalated structures were structurally characterized by SCXRD. Ag-PCM-102 was also synthesized directly via a one-pot, peri-synthetic approach. Ag-PCM-102 was found to undergo postsynthetic metal exchange with both Cu(I) and Au(I) to realize mixed-metal PCM-102 derivatives. Additionally, Cu_xAu_y -metalated PCM-102 was synthesized by sequential addition of Cu(I) and Au(I). The incorporation of low-valent metals was found to drastically increase the internal surface area of PCM-102, with these metals acting as Lewis acidic pillars to add structural integrity to the materials. Cu-,

Ag-, Au-, and $Cu_{29}Au_{71}$ -PCM-102 were evaluated for the separation of the three C_2 hydrocarbons. Interestingly, the selectivities for the different gases showed a direct dependence on the metal(s) incorporated. DFT studies of Ag-PCM-102 revealed that the selectivity observed was based on competing factors, whereby the interplay of van der Waals and moderate dipole–aryl interactions gave rise to unusual selectivity of ethane over ethylene. The materials containing Cu(I) displayed higher affinities for unsaturated hydrocarbons, indicating that the Lewis acidity of Cu plays a larger role in these systems. PCM-102 is an unusually versatile SSL platform for the utilization of low-valent metals embedded in porous MOF structures, which will allow for numerous other applications to be pursued in the near future.

EXPERIMENTAL SECTION

Materials Synthesis. PCM-102. Under an inert atmosphere, a 250 cm^3 screw-top jar was charged with tris-(4-carboxyphenyl)phosphine (0.20 g; 0.51 mmol), 4,4'-bipyridine (0.080 g; 0.51 mmol), benzoic acid (1.00 g, 8.19 mmol), and $Co(BF_4)_2 \cdot nH_2O$ (0.520 g; 1.53 mmol) dissolved in 60 cm^3 of degassed 5:2:1 DMF/MeOH/ H_2O (v/v). The mixture was sonicated for 60 s, then heated to 100 °C in a forced air oven for 24 h. The resulting large red crystals of PCM-102 were washed with fresh DMF/MeOH/ H_2O with short cycles of ultrasonic treatment to remove amorphous solids. The crystals were collected by vacuum filtration. Yield, 0.336 g. ^{31}P MAS NMR (solid, 121 MHz) δ = 5.38. Anal. calcd for $C_{54}H_{42.44}Co_3F_{0.56}N_3O_{13.44}P_2$: C, 54.1; H, 3.57; N, 3.51; F, 0.89. Found: C, 53.7; H, 3.63; N, 3.86; F, 0.88. FT-IR, ν_{max} (solid/ cm^{-1}): 476 m, 578 w, 632 m, 660 m, 698 m, 717 s, 773 s, 814 m, 838 m, 861 w, 963 w, 1015 m, 1089 m, 1181 w, 1218 w, 1253 w, 1303 w, 1387 s, 1436 w, 1488 w, 1549 m, 1603 m, 1631 s, 2798 br w, 2935 br w, 3067 br w, 3412 br w.

Ag-PCM-102; Direct Method. A reaction mixture with the same composition as described above for PCM-102, with the substitution of $AgNO_3$ (0.043 g; 0.25 mmol) for benzoic acid, was wrapped in aluminum foil and then heated at 75 °C under otherwise identical conditions. After cooling, the mother liquor was decanted, and the large red crystals were washed with degassed solvent, again using ultrasonic treatment to remove amorphous materials. Yield, 0.422 g. ^{31}P MAS NMR (solid, 121 MHz) δ = 25.15. Anal. calcd for $C_{52}H_{34.44}AgCo_3F_{0.56}N_2O_{13.44}P_2$: C, 49.6; H, 2.76; N, 2.22; F, 0.84. Found: C, 49.7; H, 3.38; N, 2.96; F, 0.85. FT-IR, ν_{max} (solid/ cm^{-1}): 478 m, 500 w, 575 w, 632 w, 659 m, 696 w, 723 m, 773 m, 781 w, 815 w, 844 w, 1014 w, 1092 m, 1180 w, 1218 w, 1251 w, 1381 s, 1487 w, 1552 br m, 1600 m, 1640 s, 2853 br w, 2924 br w, 3056 br w, 3387 br m.

Ag-PCM-102; Postsynthetic Method. Dry PCM-102 (20 mg, 0.016 mmol) and $AgNO_3$ (1.5 mg, 0.0088 mmol) were added to a 20 mL scintillation vial wrapped in aluminum foil. A 5.0 mL volume of degassed 5:2:1 DMF/MeOH/ H_2O was added in a N_2 -filled glovebag, and the vial was capped under N_2 and allowed to stand at room temperature overnight. The pink crystals were isolated by vacuum filtration and washed with degassed 5:2:1 DMF/MeOH/ H_2O , then analyzed by PXRD.

Au-PCM-102; Postsynthetic Method. Dry PCM-102 (0.075 g, 0.13 mmol P) and $(Me_2S)AuCl$ (0.021 g, 0.071 mmol) were added to a 125 mL Schlenk flask wrapped in aluminum foil under N_2 . A 15 mL volume of degassed 5:2:1 DMF/MeOH/ H_2O (v/v/v) was added via cannula. The flask was swirled periodically and allowed to stand at room temperature for 24 h. The crystals were washed with degassed 5:2:1 DMF/MeOH/ H_2O a total of 4 times, with ultrasonic treatment used to suspend any amorphous solids before decantation. The pink crystals were isolated by vacuum filtration to yield 70 mg of Au-PCM-102. ^{31}P MAS NMR (solid, 121 MHz) δ = 54.7. Anal. calcd for $C_{52}H_{34.44}AuCo_3F_{0.56}N_2O_{13.44}P_2$: C, 46.3; H, 2.57; N, 2.08. Found: C, 45.7; H, 2.79; N, 2.13.

Cu-PCM-102; Postsynthetic Method. This material was synthesized by an analogous procedure to the one used to synthesize Au-

PCM-102, but using $(\text{Me}_2\text{S})\text{CuBr}$ (0.027 g, 0.13 mmol, 1:1 P/Cu molar ratio) in place of $(\text{Me}_2\text{S})\text{AuCl}$. Pink-orange crystals were isolated by vacuum filtration to yield 67 mg of Cu-PCM-102. Anal. calcd for $\text{C}_{52}\text{H}_{34.44}\text{Co}_3\text{CuF}_{0.56}\text{N}_2\text{O}_{13.44}\text{P}_2$: C, 51.4; H, 2.87; N, 2.31. Found: C, 49.4; H, 3.25; N, 2.65.

Ag/M-PCM-102 (M = Cu, Au); Ag-Exchange Method. Dry Ag-PCM-102 (0.050 g, 0.079 mmol Ag) and $(\text{Me}_2\text{S})\text{AuCl}$ or $(\text{Me}_2\text{S})\text{-CuBr}$ (0.120 mmol) were added to a 125 cm^3 Schlenk flask under N_2 wrapped in aluminum foil. A 10 cm^3 aliquot of degassed 5:2:1 DMF/MeOH/ H_2O was added via cannula. The flask was swirled periodically and allowed to stand at room temperature for 24 h. The crystals were then isolated and cleaned using the same method described above. Recovered yield: 45–50 mg of AgAu-PCM-102 or AgCu-PCM-102.

$\text{Cu}_x\text{Au}_y\text{-PCM-102}$; Sequential Postsynthetic Addition Method. PCM-102 (0.075 g, 0.13 mmol P) and 0.55 equiv (cf. Two mmol of P) of either $(\text{Me}_2\text{S})\text{CuBr}$ or $(\text{Me}_2\text{S})\text{AuCl}$ were added to a 6 dram amber vial in a N_2 -filled glovebox, then suspended in 5 cm^3 dry DMF and left to stand for 24 h. The crystals were exchanged with fresh dry DMF three times and collected by filtration. The crystals were then added to a fresh 6 dram amber vial with the second metal precursor (0.55 equiv cf. Two mmol of P) and suspended in 5 mL of dry DMF under N_2 . After standing for 24 h, the crystals were exchanged with fresh dry DMF and collected by filtration to yield $\text{Cu}_x\text{Au}_y\text{-PCM-102}$. Addition of Cu(I) followed by addition of Au(I) gave $\text{Cu}_{29}\text{Au}_{71}\text{-PCM-102}$, while addition of Au(I) followed by Cu(I) gave $\text{Cu}_{57}\text{Au}_{43}\text{-PCM-102}$.

■ ASSOCIATED CONTENT

SI Supporting Information

The Supporting Information is available free of charge at <https://pubs.acs.org/doi/10.1021/jacs.1c05564>.

Data including additional experimental details and methods, TGA, MAS NMR, TEM, SEM-EDS, and XPS spectra, PXRD patterns, ICP-OES and BVS data, additional molecular drawings, SCXRD data and Bader charge analysis (PDF)

Accession Codes

CCDC 2081306–2081311 contain the supplementary crystallographic data for this paper. These data can be obtained free of charge via www.ccdc.cam.ac.uk/data_request/cif, or by emailing data_request@ccdc.cam.ac.uk, or by contacting The Cambridge Crystallographic Data Centre, 12 Union Road, Cambridge CB2 1EZ, UK; fax: +44 1223 336033.

■ AUTHOR INFORMATION

Corresponding Authors

Jong-San Chang – Research Center for Nanocatalysis, Korea Research Institute of Chemical Technology (KRICT), Yuseong, Daejeon 305-600, Korea; orcid.org/0000-0003-3640-8190; Email: jschang@kRICT.re.kr

Graeme Henkelman – Department of Chemistry, University of Texas at Austin, Austin, Texas 78712-0165, United States; orcid.org/0000-0002-0336-7153; Email: henkelman@utexas.edu

Simon M. Humphrey – Department of Chemistry, University of Texas at Austin, Austin, Texas 78712-0165, United States; orcid.org/0000-0001-5379-4623; Email: smh@cm.utexas.edu

Authors

R. Eric Sikma – Department of Chemistry, University of Texas at Austin, Austin, Texas 78712-0165, United States; Present Address: Department of Chemistry and Biochemistry,

University of California, San Diego, 9500 Gilman Drive, MC 0332, La Jolla, California 92093, United States

Naman Katyal – Department of Chemistry, University of Texas at Austin, Austin, Texas 78712-0165, United States

Su-Kyung Lee – Research Center for Nanocatalysis, Korea Research Institute of Chemical Technology (KRICT), Yuseong, Daejeon 305-600, Korea

Joseph W. Fryer – Austin-International Framework Undergraduate Exchange Program, College of Natural Sciences, University of Texas at Austin, Austin, Texas 78712, United States

Catherine G. Romero – Austin-International Framework Undergraduate Exchange Program, College of Natural Sciences, University of Texas at Austin, Austin, Texas 78712, United States

Samuel K. Emslie – Department of Chemistry, University of Texas at Austin, Austin, Texas 78712-0165, United States; Austin-International Framework Undergraduate Exchange Program, College of Natural Sciences, University of Texas at Austin, Austin, Texas 78712, United States

Elinor L. Taylor – Austin-International Framework Undergraduate Exchange Program, College of Natural Sciences, University of Texas at Austin, Austin, Texas 78712, United States

Vincent M. Lynch – Department of Chemistry, University of Texas at Austin, Austin, Texas 78712-0165, United States

Complete contact information is available at:

<https://pubs.acs.org/10.1021/jacs.1c05564>

Notes

The authors declare no competing financial interest.

■ ACKNOWLEDGMENTS

The authors acknowledge Dr. Hongyu Guo (ICP-OES and XPS), Dr. Shichao He (TGA), Stephanie White (SEM), and Dr. Steven Sorey (NMR) for analytical support. This work was funded by The National Science Foundation, Division of Materials Research under grant no. DMR-1905701 and the Welch Foundation (F-1738). Computational resources were provided by Extreme Science and Engineering Discovery Environment (XSEDE Allocation TG-CHE190010) and the Texas Advanced Computing Center (TACC).

■ DEDICATION

This manuscript is dedicated to the life and work of a great friend and mentor, Prof. William C. Kaska.

■ REFERENCES

- (1) (a) Yaghi, O. M.; Kalmutzki, M. J.; Dierks, C. S. *Introduction to Reticular Chemistry*; Wiley-VCH Verlag GmbH: Weinheim, 2019. (b) Yaghi, O. M.; O'Keeffe, M.; Ockwig, N. W.; Chae, H. K.; Eddaoudi, M.; Kim, J. Reticular synthesis and the design of new materials. *Nature* **2003**, *423*, 705–714. (c) Li, H.; Eddaoudi, M.; O'Keeffe, M.; Yaghi, O. M. Design and synthesis of an exceptionally stable and highly porous metal-organic framework. *Nature* **1999**, *402*, 276–279. (d) Furukawa, H.; Cordova, K. E.; O'Keeffe, M.; Yaghi, O. M. The chemistry and applications of metal-organic frameworks. *Science* **2013**, *341*, 1230444. (e) Zhou, H.-C.; Kitagawa, S. Metal-Organic Frameworks (MOFs). *Chem. Soc. Rev.* **2014**, *43*, 5415–5418. (f) Howarth, A. J.; Liu, Y.; Li, P.; Li, Z.; Wang, T. C.; Hupp, J. T.; Farha, O. K. Chemical, thermal and mechanical stabilities of metal-organic frameworks. *Nat. Rev. Mater.* **2016**, *1*, 15018.
- (2) (a) Li, J.-R.; Kuppler, R. J.; Zhou, H.-C. Selective gas adsorption and separation in metal-organic frameworks. *Chem. Soc. Rev.* **2009**, *38*,

- 1477–1504. (b) Bloch, E. D.; Queen, W. L.; Krishna, R.; Zadrozny, J. M.; Brown, C. M.; Long, J. R. Hydrocarbon Separations in a Metal-Organic Framework with Open Iron(II) Coordination Sites. *Science* **2012**, *335*, 1606–1610. (c) Yang, X.; Xu, Q. Bimetallic Metal-Organic Frameworks for Gas Storage and Separation. *Cryst. Growth Des.* **2017**, *17*, 1450–1455. (d) Zhao, X.; Wang, Y.; Li, D.-S.; Bu, X.; Feng, P. Metal-Organic Frameworks for Separation. *Adv. Mater.* **2018**, *30*, 1705189.
- (3) (a) Jiao, L.; Wang, Y.; Jiang, H.-L.; Xu, Q. Metal-Organic Frameworks as Platforms for Catalytic Applications. *Adv. Mater.* **2018**, *30*, 1703663. (b) Drake, T.; Ji, P.; Lin, W. Site Isolation in Metal-Organic Frameworks Enables Novel Transition Metal Catalysis. *Acc. Chem. Res.* **2018**, *51*, 2129–2138. (c) Qin, J.-S.; Yuan, S.; Lollar, C.; Pang, J.; Alsalmeh, A.; Zhou, H.-C. Stable metal-organic frameworks as a host platform for catalysis and biomimetics. *Chem. Commun.* **2018**, *54*, 4231–4249. (d) Rimoldi, M.; Howarth, A. J.; DeStefano, M. R.; Lin, L.; Goswami, S.; Li, P.; Hupp, J. T.; Farha, O. K. Catalytic Zirconium/Hafnium-Based Metal-Organic Frameworks. *ACS Catal.* **2017**, *7*, 997–1014.
- (4) (a) Bloch, E. D.; Britt, D. L.; Lee, C.; Doonan, C. J.; Uribe-Romo, F. J.; Furukawa, H.; Long, J. R.; Yaghi, O. M. Metal Insertion in a Microporous Metal-Organic Framework Lined with 2,2'-Bipyridine. *J. Am. Chem. Soc.* **2010**, *132*, 14382–14384. (b) Lin, R.-B.; Xiang, S.; Zhou, W.; Chen, B. Microporous Metal-Organic Framework Materials for Gas Separation. *Chem.* **2020**, *6*, 337–363. (c) Xiao, D. J.; Gonzalez, M. I.; Darago, L. E.; Vogiatzis, K. D.; Haldoupis, E.; Gagliardi, L.; Long, J. R. Selective, Tunable O₂ Binding in Cobalt(II)-Triazolate/Pyrazolate Metal-Organic Frameworks. *J. Am. Chem. Soc.* **2016**, *138*, 7161–7170.
- (5) (a) McDonald, T. M.; Mason, J. A.; Kong, X.; Bloch, E. D.; Gygi, D.; Dani, A.; Crocella, V.; Giordanino, F.; Odoh, S. O.; Drisdell, W.; Vlaisavljevich, B.; Dzubak, A. L.; Poloni, R.; Schnell, S. K.; Planas, N.; Lee, K.; Pascal, T.; Wan, L. F.; Prendergast, D.; Neaton, J. B.; Smit, B.; Kortright, J. B.; Gagliardi, L.; Bordiga, S.; Reimer, J. A.; Long, J. R. Cooperative insertion of CO₂ in diamine-appended metal-organic frameworks. *Nature* **2015**, *519*, 303–308. (b) Rosen, A. S.; Mian, M. R.; Islamoglu, T.; Chen, H.; Farha, O. K.; Notestein, J. M.; Snurr, R. Q. Tuning the Redox Activity of Metal-Organic Frameworks for Enhanced, Selective O₂ Binding: Design Rules and Ambient Temperature O₂ Chemisorption in a Cobalt-Triazolate Framework. *J. Am. Chem. Soc.* **2020**, *142*, 4317–4328. (c) Haraguchi, T.; Otsubo, K.; Sakata, O.; Fujiwara, A.; Kitagawa, H. Guest-Induced Two-Way Structural Transformation in a Layered Metal-Organic Framework Thin Film. *J. Am. Chem. Soc.* **2016**, *138*, 16787–16793.
- (6) (a) Agnew, D. W.; DiMucci, I. M.; Arroyave, A.; Gembicky, M.; Moore, C. E.; MacMillan, S. N.; Rheingold, A. L.; Lancaster, K. M.; Figueroa, J. S. Crystalline Coordination Networks of Zero-Valent Metal Centers: Formation of a 3-Dimensional Ni(0) Framework with *m*-Terphenyl Diosocyanides. *J. Am. Chem. Soc.* **2017**, *139*, 17257–17260. (b) Jeoung, S.; Kim, S.; Kim, M.; Moon, H.-R. Pore Engineering of Metal-Organic Frameworks with Coordinating Functionalities. *Coord. Chem. Rev.* **2020**, *420*, 213377.
- (7) (a) Ding, M.; Cai, X.; Jiang, H.-L. Improving MOF stability: approaches and applications. *Chem. Sci.* **2019**, *10*, 10209–10230. (b) Yuan, S.; Feng, L.; Wang, K.; Pang, J.; Bosch, M.; Lollar, C.; Sun, Y.; Qin, J.; Yang, X.; Zhang, P.; Wang, Q.; Zou, L.; Zhang, Y.; Zhang, L.; Fang, Y.; Li, J.; Zhou, H.-C. Stable Metal-Organic Frameworks: Design, Synthesis, and Applications. *Adv. Mater.* **2018**, *30*, 1704303. (c) Colombo, V.; Galli, S.; Choi, H. J.; Han, G. D.; Maspero, A.; Palmisano, G.; Masciocchi, N.; Long, J. R. High thermal and chemical stability in pyrazolate-bridged metal-organic frameworks with exposed metal sites. *Chem. Sci.* **2011**, *2*, 1311–1319. (d) Lv, X.-L.; Wang, K.; Wang, B.; Su, J.; Zou, X.; Xie, Y.; Li, J.-R.; Zhou, H.-C. A Base-Resistant Metalloporphyrin Metal-Organic Framework for C–H Bond Halogenation. *J. Am. Chem. Soc.* **2017**, *139*, 211–217. (e) Park, K. S.; Ni, Z.; Cote, A. P.; Choi, J. Y.; Huang, R.; Uribe-Romo, F. J.; Chae, H. K.; O’Keeffe, M.; Yaghi, O. M. Exceptional chemical and thermal stability of zeolitic imidazolate frameworks. *Proc. Natl. Acad. Sci. U. S. A.* **2006**, *103*, 10186–10191.
- (8) Muldoon, P. F.; Liu, C.; Miller, C. C.; Koby, S. B.; Gamble Jarvi, A.; Luo, T.-Y.; Saxena, S.; O’Keeffe, M.; Rosi, N. L. Programmable Topology in New Families of Heterobimetallic Metal-Organic Frameworks. *J. Am. Chem. Soc.* **2018**, *140*, 6194–6198.
- (9) (a) Doonan, C. J.; Morris, W.; Furukawa, H.; Yaghi, O. M. Isoreticular Metalation of Metal-Organic Frameworks. *J. Am. Chem. Soc.* **2009**, *131*, 9492–9493. (b) Oisaki, K.; Li, Q.; Furukawa, H.; Czaja, A. U.; Yaghi, O. M. A Metal-Organic Framework with Covalently Bound Organometallic Complexes. *J. Am. Chem. Soc.* **2010**, *132*, 9262–9264.
- (10) (a) Fei, H.; Cohen, S. M. A robust, catalytic metal-organic framework with open 2,2'-bipyridine sites. *Chem. Commun.* **2014**, *50*, 4810–4812. (b) Fei, H.; Shin, J.; Meng, Y. S.; Adelman, M.; Sutter, J.; Meyer, K.; Cohen, S. M. Reusable Oxidation Catalysis Using Metal-Monocatecholato Species in a Robust Metal-Organic Framework. *J. Am. Chem. Soc.* **2014**, *136*, 4965–4973.
- (11) (a) Burgun, A.; Crees, R. S.; Cole, M. L.; Doonan, C. J.; Sumbly, C. J. A 3-D diamondoid MOF catalyst based on *in situ* generated [Cu(L)] N-heterocyclic carbene (NHC) linkers: hydroboration of CO₂. *Chem. Commun.* **2014**, *50*, 11760–11763. (b) Evans, J. D.; Sumbly, C. J.; Doonan, C. J. Post-synthetic metalation of metal-organic frameworks. *Chem. Soc. Rev.* **2014**, *43*, 5933–5951. (c) Young, R. J.; Huxley, M. T.; Pardo, E.; Champness, N. R.; Sumbly, C. J.; Doonan, C. J. Isolating reactive metal-based species in Metal-Organic Frameworks – viable strategies and opportunities. *Chem. Sci.* **2020**, *11*, 4031–4050.
- (12) (a) Dunning, S. G.; Nandra, G.; Conn, A. D.; Chai, W.; Sikma, R. E.; Lee, J. S.; Kunal, P.; Reynolds, J. E., III; Chang, J.-S.; Steiner, A.; Henkelman, G.; Humphrey, S. M. A Metal-Organic Framework with Cooperative Phosphines That Permit Post-Synthetic Installation of Open Metal Sites. *Angew. Chem., Int. Ed.* **2018**, *57*, 9295–9299. (b) Nuñez, A. J.; Shear, L. N.; Dahal, N.; Ibarra, I. A.; Yoon, J.; Hwang, Y. K.; Chang, J.-S.; Humphrey, S. M. A coordination polymer of (Ph₃P)AuCl prepared by post-synthetic modification and its application in 1-hexene/n-hexane separation. *Chem. Commun.* **2011**, *47*, 11855–11857. (c) Dunning, S. G.; Reynolds, J. E., III; Walsh, K. M.; Kristek, D. J.; Lynch, V. M.; Kunal, P.; Humphrey, S. M. Direct, One-Pot Syntheses of MOFs Decorated with Low-Valent Metal-Phosphine Complexes. *Organometallics* **2019**, *38*, 3406–3411.
- (13) Sikma, R. E.; Kunal, P.; Dunning, S. G.; Reynolds, J. E., III; Lee, J. S.; Chang, J.-S.; Humphrey, S. M. Organoarsine Metal-Organic Framework with *cis*-Diarsine Pockets for the Installation of Uniquely Confined Metal Complexes. *J. Am. Chem. Soc.* **2018**, *140*, 9806–9809.
- (14) Sawano, T.; Thacker, N. C.; Lin, Z.; McIsaac, A. R.; Lin, W. Robust, Chiral, and Porous BINAP-Based Metal-Organic Frameworks for Highly Enantioselective Cyclization Reactions. *J. Am. Chem. Soc.* **2015**, *137*, 12241–12248.
- (15) Bohnsack, A. M.; Ibarra, I. A.; Bakhmutov, V. I.; Lynch, V. M.; Humphrey, S. M. Rational Design of Porous Coordination Polymers Based on Bis(phosphine)MCl₂ Complexes That Exhibit High-Temperature H₂ Sorption and Chemical Reactivity. *J. Am. Chem. Soc.* **2013**, *135*, 16038–16041.
- (16) (a) He, J.; Waggoner, N. W.; Dunning, S. G.; Steiner, A.; Lynch, V. M.; Humphrey, S. M. A PCP Pincer Ligand for Coordination Polymers with Versatile Chemical Reactivity: Selective Activation of CO₂ Gas over CO Gas in the Solid State. *Angew. Chem., Int. Ed.* **2016**, *55*, 12351–12355. (b) Burgess, S. A.; Kassie, A.; Baranowski, S. A.; Fritzsche, K. J.; Schmidt-Rohr, K.; Brown, C. M.; Wade, C. R. Improved Catalytic Activity and Stability of a Palladium Pincer Complex by Incorporation into a Metal-Organic Framework. *J. Am. Chem. Soc.* **2016**, *138*, 1780–1783.
- (17) Humphrey, S. M.; Allan, P. K.; Oungoulian, S. E.; Ironside, M. S.; Wise, E. R. Metal-organophosphine and metal-organophosphonium frameworks with layered honeycomb-like structures. *Dalton Trans.* **2009**, 2298–2305.
- (18) Bordwell, F. G. Equilibrium Acidities in Dimethyl Sulfoxide Solution. *Acc. Chem. Res.* **1988**, *21*, 456–463.
- (19) Boeré, R. T.; Zhang, Y. Extremely bulky triarylphosphines incorporating 2,6-diisopropylphenyl substituents; consideration of

steric shielding and steric pressure. *J. Organomet. Chem.* **2005**, *690*, 2651–2657.

(20) Farha, O. K.; Hupp, J. T. Rational Design, Synthesis, Purification, and Activation of Metal-Organic Framework Materials. *Acc. Chem. Res.* **2010**, *43*, 1166–1175.

(21) Barron, P. F.; Dyason, J. C.; Healy, P. C.; Engelhardt, L. M.; Skelton, B. W.; White, A. H. Lewis base adducts of Group 11 metal compounds. Part 24. Co-ordination of triphenylphosphine with silver nitrate. A solid-state cross-polarization magic angle spinning ^{31}P nuclear magnetic resonance, crystal structure, and infrared spectroscopic study of $\text{Ag}(\text{PPh}_3)_n\text{NO}_3$ ($n = 1-4$). *J. Chem. Soc., Dalton Trans.* **1986**, 1965–1970.

(22) Bachman, R. E.; Andretta, D. F. Metal-Ligand Bonding in Coinage Metal-Phosphine Complexes: The Synthesis and Structure of Some Low-Coordinate Silver(I)-Phosphine Complexes. *Inorg. Chem.* **1998**, *37*, 5657–5663.

(23) Strauss, S. H. The search for larger and more weakly coordinating anions. *Chem. Rev.* **1993**, *93*, 927–942.

(24) CCDC reference codes: IDIXAX, MIJWUA, RIJCAR, ASIZUX, BEWROK, KUXDOW, PAWGUP, SEGBUE, SUFVOE, TEYBOO, XAYQOE, XAYQUK, XAYRAR, CISYIP, WOCZEW.

(25) Horike, S.; Shimomura, S.; Kitagawa, S. Soft porous crystals. *Nat. Chem.* **2009**, *1*, 695–704.

(26) Li, J.-R.; Yu, J.; Lu, W.; Sun, L.-B.; Sculley, J.; Balbuena, P. B.; Zhou, H.-C. Porous materials with pre-designed single-molecule traps for CO_2 selective adsorption. *Nat. Commun.* **2013**, *4*, 1538.

(27) CCDC reference codes: ACPHCU, ACPHCU01, ACPHCU02, BEMZEA, BIBQAG, BIZPUV, BOMFUE, CEFTOX, CERTOI, CERTOI10, COBJAE, COTGIB, DIRJIX, DOKQEZ, DULTIO, DUYDOR, DUYDUX, EDAHEW, FIKREZ, GINLOG, GINMAT, GINMEX, GUXJOZ, HIBPUD, HICHOQ, HICLEK, HICLIO, HICLOU, HUYTAW, IJOHUL, ITADIS, JOCDIQ, KEMLAP, KEMLAP01, KILPUT, KILQAA, KILQEE, KILQOO, KILQUU, KISVUG, LESMIF, LOHLOK, MUMCOM, NENPEB, NIJSOO, NITPPC01, NITPPC02, NITPPC20, NITPCC21, NITPCC22, NITPCC23, NOQSES, NTOLCU, NUNZUS, REHKEU, REPXIU, RUNREX, SIWYAZ, TIZJUH, TOCQOR, TODNAB, TODNEF, TODNIJ, TOLVUM, TUKVIE, UNAVAG, WEPJEG, WEPJIK, WEPKAD, WINCII, WUPLUP, YECCIT, YECCOZ, YECDAM, YEFVEN, ZACZUY.

(28) CCDC reference codes: BARBUT, BUJXEJ, GACRAD, GORNIM, HINRUT, IMJEU, KASXUX, KASXUX01, KEJYAB, QICVOO, SOSTAV, SUBSIT, TEZYOO, UXITUS, VUXHED, WABPIY, WABPOE, WAGFUH, WAGFUH01, WEVZAY, WEVZAY01, WIMLUA, ZEPYIC, ZOZMEG.

(29) (a) Kobayashi, A.; Komatsu, K.; Ohara, H.; Kamada, W.; Chishina, Y.; Tsuge, K.; Chang, H.-C.; Kato, M. Photo- and Vapor-Controlled Luminescence of Rhombic Dicopper(I) Complexes Containing Dimethyl Sulfoxide. *Inorg. Chem.* **2013**, *52*, 13188–13198. (b) Müller, T. E.; Choi, S. W. -K.; Mingos, D. M. P.; Murphy, D.; Williams, D. J.; Yam, V. W. -W. Synthesis, structural characterization and photophysical properties of ethyne-gold(I) complexes. *J. Organomet. Chem.* **1994**, *484*, 209–224.

(30) (a) Cohen, S. M. The Postsynthetic Renaissance in Porous Solids. *J. Am. Chem. Soc.* **2017**, *139*, 2855–2863. (b) Kim, M.; Cahill, J. F.; Fei, H.; Prather, K. A.; Cohen, S. M. Postsynthetic Ligand and Cation Exchange in Robust Metal-Organic Frameworks. *J. Am. Chem. Soc.* **2012**, *134*, 18082–18088.

(31) (a) Safarik, D. J.; Eldridge, R. B. Olefin/Paraffin Separations by Reactive Absorption: A Review. *Ind. Eng. Chem. Res.* **1998**, *37*, 2571–2581. (b) Padin, J.; Yang, R. T. New sorbents for olefin/paraffin separations by adsorption via π -complexation: synthesis and effects of substrates. *Chem. Eng. Sci.* **2000**, *55*, 2607–2616.

(32) Mukherjee, S.; Sensharma, D.; Chen, K.-J.; Zaworotko, M. J. Crystal engineering of porous coordination networks to enable separation of C_2 hydrocarbons. *Chem. Commun.* **2020**, *56*, 10419–10441.

(33) (a) Li, J.; Han, X.; Kang, X.; Chen, Y.; Xu, S.; Smith, G. L.; Tillotson, E.; Cheng, Y.; McCormick McPherson, L. J.; Teat, S. J.;

Rudic, S.; Ramirez-Cuesta, A. J.; Haigh, S. J.; Schröder, M.; Yang, S. Purification of propylene and ethylene by a robust metal-organic framework mediated by host-guest interactions. *Angew. Chem., Int. Ed.* **2021**, *60*, 15541–15547. (b) Lee, S.-K.; Park, H.; Yoon, J. W.; Kim, K.; Cho, S. J.; Maurin, G.; Ryoo, R.; Chang, J.-S. Microporous 3D Graphene-like Zeolite-Templated Carbons for Preferential Adsorption of Ethane. *ACS Appl. Mater. Interfaces* **2020**, *12*, 28484–28495. (c) Pires, J. O.; Pinto, M. S. L.; Saini, V. K. Ethane selective IRMOF-8 and its significance in ethane–ethylene separation by adsorption. *ACS Appl. Mater. Interfaces* **2014**, *6*, 12093–12099. (d) Lin, R.-B.; Wu, H.; Li, L.; Tang, X.-L.; Li, Z.; Gao, J.; Cui, H.; Zhou, W.; Chen, B. Boosting ethane/ethylene separation within isoreticular ultramicroporous metal–organic frameworks. *J. Am. Chem. Soc.* **2018**, *140*, 12940–12946.

(34) Myers, A. L. Equation of State for Adsorption of Gases and their Mixtures in Porous Materials. *Adsorption* **2003**, *9*, 9–16.